

Quantifying the Susceptibility of 316H and 347H to Reheat-Type Cracking

Notched bar tests were a reliable method to assess susceptibility; 347H was more prone to cracking, and failure times correlated with the precipitation of intragranular Nb(C,N)

BY G. A. YOUNG, A. BRITTAN, A. DONG, K. CHEN, AND N. NGUYEN

Abstract

Notched-bar stress relaxation tests were conducted on samples machined from the heat-affected zones of 347H and 316H V-groove weldments fabricated with 16-8-2 filler metal. Tests were performed between 500–650°C with two different notch radii to compare the performance of the alloys. Samples were loaded to target stress, held in stroke control for 500 h and then reloaded to the target stress for additional cycles until failure or the test was ended. Post-test, the samples were characterized by light optical and scanning electron microscopy. Results showed that this test method is a repeatable and sensitive method to produce intergranular cracking in austenitic stainless steels. Both alloys showed resistance to cracking at 500°C and susceptibility at 550°C but diverged in behavior at 600°C, where the 347H weldments showed increased susceptibility and the 316H weldments showed increased resistance. Failure times and temperatures in 347H correlated with the formation of intragranular Nb(C,N), and analysis indicated that precipitation-induced strains promoted cracking in 347H. The ability to control the stress state, creep damage and microstructure tested and produce intergranular cracking at temperatures prototypical of operation are key advantages of this test method, which should be adopted as a standard to facilitate mechanistic understanding and develop mitigation strategies for reheat-type cracking.

Keywords

- Reheat Cracking
- Stress Relaxation Cracking
- Ductility Dip Cracking
- Austenitic Stainless Steels
- Weldability

Introduction

Stress relaxation cracking in austenitic alloys is of significant interest to the power generation, chemical process, oil & gas, and other industries where operating temperatures > 450°C place many alloys in a regime of susceptibility (Refs. 1–8). This paper defines stress relaxation cracking as the initiation of intergranular failure (i.e., the initiation of intergranular creep cracking) to separate the phenomenon from other weldability issues and creep crack growth. Additionally, this work was focused on attempting to quantify and better understand the susceptibility of different grades of austenitic stainless steels to this phenomenon.

Overview of the Phenomenon

Several authors have discussed the similarities in intergranular cracking that occurs in austenitic alloys at intermediate homologous temperatures in welds, heat-affected zones, and base metals (Refs. 2, 9–11). In trying to understand those phenomena, the timescale to produce cracking, the temperature regime that cracking occurs in, and the associated phase transformations are key considerations. Upon review of the welding literature, grouping these phenomena into three distinct timescales helps rationalize why different terminologies have developed.

Ductility dip cracking (DDC). This refers to intergranular cracking associated with a significant loss in uniaxial tensile ductility. Thus, DDC occurs at the timescales of typical hot

<https://doi.org/10.29391/2025.104.021>

Reheat-Type Cracking Time Scales

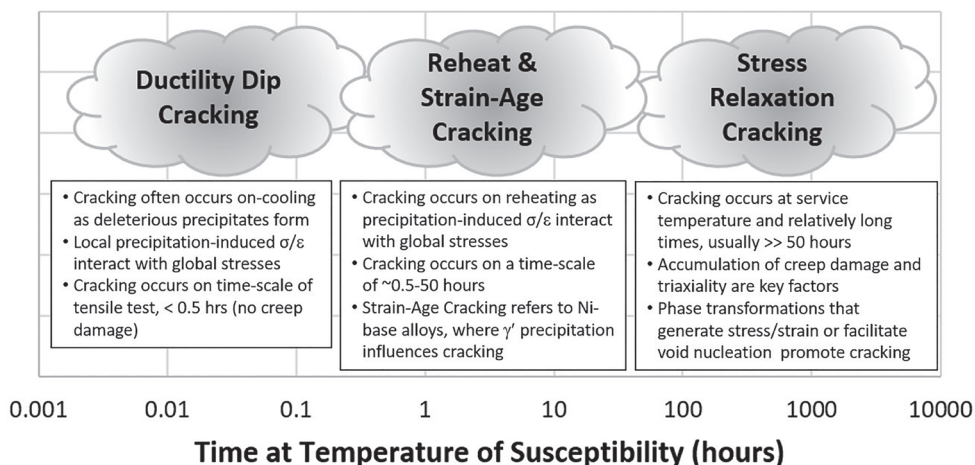


Fig. 1 – Illustration of the typical time regimes of ductility dip, reheat, and stress relaxation cracking. At short timescales, global and precipitation-induced stresses control cracking (ductility dip cracking), while creep damage plays a larger role at long times (stress relaxation cracking).

tensile testing, usually significantly < 0.5 h at temperature and often on-cooling as second phases form in the heat-affected zone. Young et al. (Ref. 10) have assessed a large body of DDC literature and performed testing on Ni-30Cr alloys where this phenomenon is coversion in multipass welds. That work showed that DDC is typically associated with the precipitation of a coherent or partially coherent phase that produces a local precipitation-induced stress and a more-global stress (e.g., from a restrained or constrained dissimilar metal weld) (Ref. 10). At these timescales, the accumulation of creep damage is minimal, and cracking requires the presence of both global and local precipitation-induced stresses.

Reheat cracking and strain-age cracking describe failure phenomena associated with post-weld heat treatments or short times at operating temperature and typically occur on timescales of 0.5–50 h. Here, global stresses in the component play a role; triaxial stresses may promote degradation, and phase transformations may also have a key contribution. For example, as discussed in Ref. 12, γ' prime strengthened alloys that produce tension between precipitates at short times are most susceptible to cracking. Because the misfit strain between the γ' (or γ'') and the matrix is composition-dependent, strain-age cracking is notably composition-dependent.

Stress relaxation cracking encompasses the failure phenomenon associated with the accumulation of creep damage in a regime where the alloy exhibits degraded creep ductility and typically occurs at times $\gg 50$ h. Global and precipitation-induced stresses can have contributory roles, but cracking in components is often the result of accumulated creep damage in a time/temperature regime associated with low creep ductility. Here, triaxial stresses are a key factor that lowers the creep failure ductility, and conditions of high elastic follow-up promote the accumulation of creep damage. Precipitation may either produce a local stress or strain or result in a locally weak zone (e.g., a precipitate-de-

nuded zone), which can localize creep damage and promote cracking.

With this view, we define “reheat-type cracking” as the general phenomenon that encompasses these sub-modes: ductility dip, strain-age, reheat, and stress relaxation, as illustrated in Fig. 1. In addition to the description of each cracking sub-mode above, we note that several complex metallurgical factors can influence cracking, including:

- Phase transformations that induce internal stress or strain,
- Precipitation of second phases, which degrade ductility,
- Development of microstructures that localize deformation,
- Segregation of embrittling elements to interfaces that nucleate cracking, and
- Plastic strain, which increases hardness and reduces ductility and toughness.

Selection of a Test Method

Given the classification of cracking modes above, the choice of test method to assess degradation requires careful consideration to assess the performance of components accurately. Since cracking can be strongly affected by both mechanical and metallurgical factors, the test method should simulate the appropriate stress states, microstructure, and in-service changes that affect cracking (e.g., precipitation and segregation). For example, triaxial stresses and creep damage accumulation are critical factors in producing stress relaxation cracking in austenitic stainless steels (Refs. 13, 14). At the same time, gamma prime precipitation is a critical factor in strain-age cracking (Refs. 10, 12, 15–17).

A summary of tests used to assess cracking is given in Table 1, which compares the test against some key mechanical and metallurgical conditions.

- Weld mockups are often the most prototypical method to assess component performance but can suffer from difficulty in reproducing the restraint/constraint of actual

Table 1 – Comparison of Test Methods Used to Investigate Reheat-Type Cracking

Test Type	Mechanical Conditions			Metallurgical Conditions			References
	Control of Triaxiality	Elastic Follow-Up $1 < Z < \infty$	Well Characterized Stress State	Samples Appropriate Microstructure	Prototypical Test Temperature	Test Duration	
Weld Mockup	Limited	Variable	Usually not	Yes	Yes	Usually typical of service	Refs. 18–24
C-Ring	Possible	1	Usually not	Possible but difficult for heavy section welds	Yes	Dependent on stress and temperature	Refs. 25, 26
Bending (Displacement)	No	1	Usually not	Possible	Yes	Dependent on stress and temperature	Refs. 4, 27, 28
Bending (Load)	No	∞	Usually not	Possible	Yes	Dependent on stress and temperature	Refs. 27, 29, 30
Uniaxial Tension	No	Variable	Yes	Possible	Yes	Typically accelerated	Refs. 2, 31
Constant Load Creep Rupture	Possible	∞	Yes	Possible	Yes	Typically accelerated	Refs. 32–36
Gleeble Based	Typically uniaxial but Messler and Li used notched bars	Variable	Yes	Possible	Possible but higher temperatures often used	Typically accelerated	Refs. 13, 17, 37–40
Fracture Mechanics-Type	High triaxiality	$Z > 1$ simulated by reloading	Yes	Possible but small in extent	Yes	Typically accelerated	Refs. 35, 41–47
Uniaxial/ Notched Bar Stress Relaxation	Yes	$Z > 1$ varies with notch geometry and simulated by reloading	Yes	Possible	Yes	Prototypical or accelerated with higher stress or frequent reloading	Refs. 14, 48–50, and this work

components, and characterization of the resulting stress state may require time-consuming and expensive weld residual stress measurements. If manual welding is used, this can introduce another variable that is difficult to control. Despite these limitations, mockups such as the Borland Mockup have been successful in reproducing in-service cracking.

- C-ring tests. These samples can be machined from an actual weldment but may not be suitable for heavy-section welds.

Tests are typically performed under constant displacement such that there is no elastic follow-up. Triaxiality can be introduced with a notch, but it may be hard to assess a wide range of stress states.

- Bend tests can be performed under constant displacement or constant load. Constant displacement tests may be non-conservative unless the sample is reloaded to simulate elastic

Table 2 – Weighted Ranking of Tests Used to Assess Reheat-Type Cracking

Test Type	Mechanical Conditions			Metallurgical Conditions			Other		Rank [‡]
	Control of Triaxiality	$1 < Z^* < \infty$	Well Characterized Stress State	Samples Appropriate Microstructure	Prototypical Test Temperature	Test Duration	Run Tests in Parallel	Quantitative	
Importance	5	5	4	5	5	5	4	4	
Gleeble-Based	3	3	5	4	3	2	1	3	107
Bending-Displacement	2	2	2	4	5	3	5	2	112
Bending-Load Control	2	2	2	4	5	3	5	2	112
C-Ring	3	2	2	4	4	4	5	3	121
Uniaxial Tension	1	1	5	4	5	3	5	4	122
Fracture Mechanics Type	2	5	4	2	4	4	5	4	135
Constant Load Creep	5	1	5	4	4	3	5	4	137
Weld Mockup	3	2	3	5	5	5	5	3	139
Notched Bar Stress Relaxation	5	5	5	4	5	5	5	5	176

*Where Z is the elastic follow-up factor; ‡Rank = Σ (Importance x Score)

follow-up, while constant load testing is overly severe for many components.

- Uniaxial tensile tests. Isothermal tensile tests, sometimes at slow stroke rates, have been used to assess reheat cracking susceptibility in simulated heat-affected zones and on samples machined from weldments.

- Constant load creep-rupture testing can control triaxiality via the sample notch radius, but testing occurs at one extreme of mechanical loading. Samples can be heat-treated or machined from weldments to obtain the metallurgical structure of interest. However, constant load tests may not accurately represent the accumulation of creep damage at low strain rates. See “stress relaxation tests.”

- Gleeble-based tests allow in-situ heat treatment of the test sample to simulate the desired metallurgical structure of interest. Triaxiality can be controlled via the use of notched

samples, but this adds difficulty in controlling the temperature in the reduced section. Gleeble-based testing is often accelerated by testing at high temperatures and/or under mechanically severe loading to minimize test durations, factors that may not represent service exposure.

- Fracture-mechanics-type tests use sharp notches and sometimes pre-compression to induce high, triaxial residual stresses. Cracking can occur as creep damage accumulates in front of the notch tip.

- Stress relaxation tests. These uniaxial, notched samples can control triaxiality via the notch radius, and elastic follow-up is simulated by reloading. Samples can be machined from a metallurgical structure of interest, and cracking can be produced at prototypical test temperatures and times. With the ability to control these key variables, notched bar stress relaxation tests provide a basis to fairly compare the risk of

Ranking of Methods to Assess Stress Relaxation Cracking

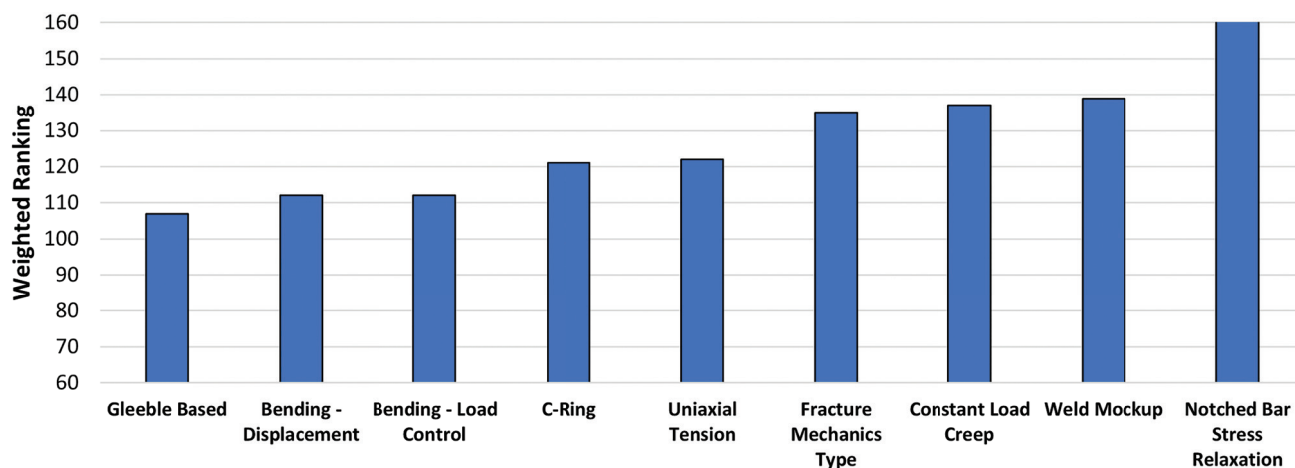


Fig. 2 — Comparison of the weighted ranking of stress relaxation test methods. In this assessment, the ability to control triaxiality, simulate elastic follow-up, and produce cracking in the time/temperature regime observed in service are key advantages of the notch bar stress relaxation method.

Table 3 — Summary of Material Compositions Used in This Study

	Cr	Ni	Mo	Mn	C	N	Si	P	S	Nb	Other*
347H HT 315523	17.5	9.07	0.019	1.45	0.046	—	0.468	0.025	0.0008	0.46	YS 256 MPa 53% El
16-8-2 HT 588311 Lot YT0974	15.6	8.0	1.3	1.50	0.04	0.047	0.47	0.02	< 0.001	0.08	3 FN (WRC)
316H HT N19658	17.3	11.4	2.4	1.36	0.063	0.054	0.425	0.018	0.003	—	YS 270 MPa 65% El

*Here, YS is the 0.2% yield strength, % El is the tensile elongation, and FN (WRC) is the ferrite number as defined from the Welding Research Council diagram.

stress relaxation cracking in existing alloys and to establish susceptibility in novel alloys where component experience is not established. The disadvantages of this test method include potentially long testing times and the need for expensive servo-controlled mechanical testing systems. However, tests can be run in parallel and potentially accelerated via high triaxiality, high net section stress, and/or frequent reloading. The appropriate testing conditions should factor in component service conditions and the relevant time-temperature-transformation diagram to ensure similitude. In this work, we have chosen to replicate the test procedure of Spindler and Smith to facilitate direct comparison with their results (Ref. 14).

Given the wide range of tests and thermo-mechanical conditions used to assess reheat-type cracking in Table 1, the selection of an appropriate test method or methods is chal-

lenging. To better assess test selection, a weighted ranking is presented in Table 2, where the importance of each factor is assigned a number between 5 (critically important to the test) and 1 (desired but not technically critical), as well as a score between 5 (fully meets requirement) to 1 (poor fulfillment of the requirement). The sum of the weighted rankings (Equation 1) is the overall ranking shown in Fig. 2. In the authors' judgement, since the sub-mode of cracking of interest in this work is stress relaxation cracking, the ability to precisely control the triaxiality of the test, to simulate the elastic follow-up, to sample the microstructure of interest, and to produce intergranular cracking in a time-temperature regime that is prototypical of field component experience are critical factors and were assigned an importance of 5. Similarly, the ability of the test to be conducted with a well-characterized stress state, to run tests in parallel (without prohibitive

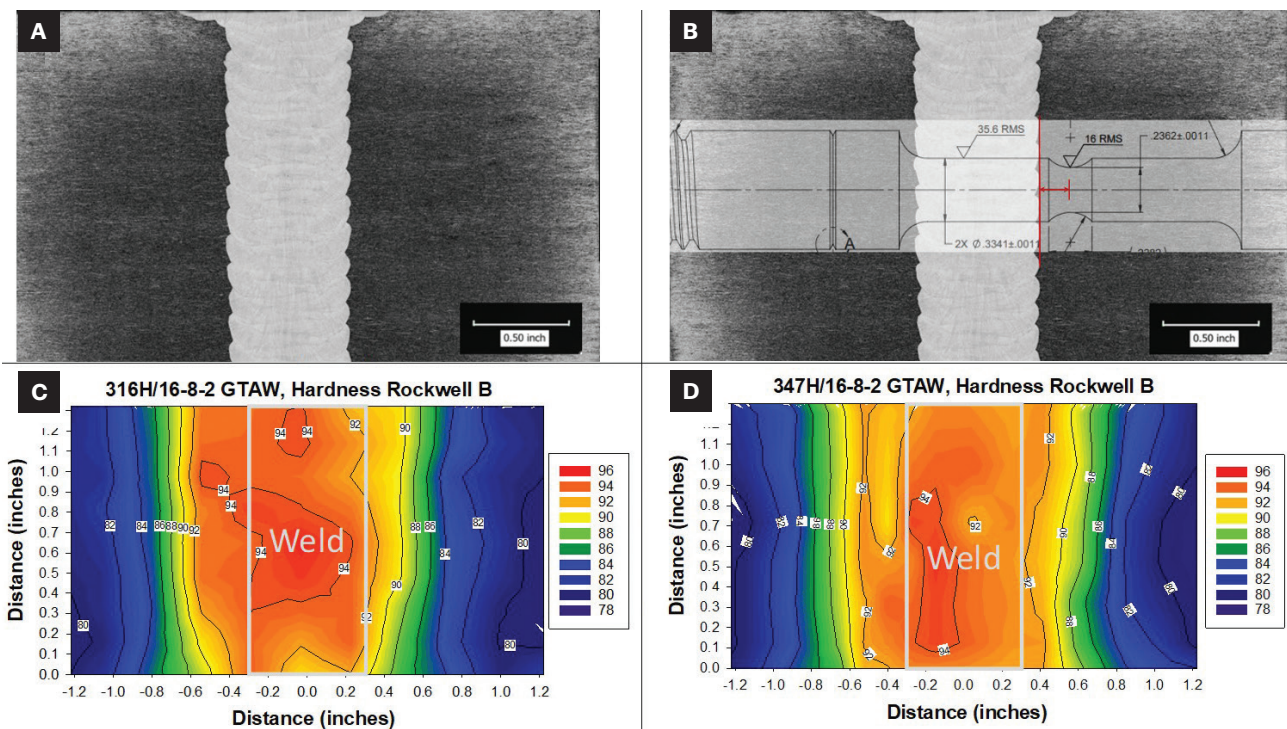


Fig. 3 – Macrographs of the narrow groove GTAW used in this study: A – A macrograph of the 316H/16-8-2 weld; B – an illustration of the layout of the extracted samples relative to the weld fusion line. Hardness maps for C – 316H/16-8-2 and D – 347H/16-8-2. The weld fusion region spans from approximately -0.3 to $+0.3$ in., and the sample notches were centered at $+0.157$ in. from the fusion line in a region of ~ 89 – 91 HRB.

Table 4 – Welding Parameters Used to Fabricate the Hot Wire, Narrow Groove, Gas Tungsten Arc Weldments

Parameter	Value
Current	325 A
Voltage	11.1 V
Travel Speed	6.25 in./min
Shielding Gas	75% Ar–25% He
Nominal Heat Input	34.6 kJ/in.

cost), and to have clear, quantifiable metrics (such as time to crack initiation) are very important factors and were given an importance of 4.

$$\text{Test Ranking} = \sum (\text{Importance}) * (\text{Score}) \quad (1)$$

Specifically for stress relaxation and reheat cracking/strain-age cracking, there is concern that accelerated tests (via high temperature and imposed fast stroke rates relative

to creep deformation, etc.) could miss important factors, such as the accumulation of creep damage, precipitation of deleterious second phases, and microsegregation of embrittling elements. Similarly, tests conducted under constant displacement or in uniaxial tension may be too innocuous and fail to trigger stress relaxation cracking (Ref. 7). Thus, Gleeble-based tests, bending, and C-ring-type tests were ranked relatively low, and fracture mechanics-based and creep-type tests were ranked higher. Weld mockups were also ranked high for their prototypical nature, but we noted the potential difficulty in controlling and characterizing the residual stress state and the limited ability to assess the instance and degree of cracking quantitatively. For these reasons, we chose notched bar stress relaxation testing (Ref. 14) to assess the stress relaxation cracking resistance of the 347H and 316H heat-affected zones.

Experimental Procedure

Restrained, narrow-groove, hot-wire, gas tungsten arc welds (GTAW) were fabricated from 2-in. plates (either 347H or 316H) and 16-8-2 weld filler metal. The compositions of the plate and weld wire used in these tests are given in Table 3, and the nominal welding parameters are given in Table 4. The narrow-groove joint used a 1 deg bevel and two passes per layer, which resulted in 35 beads per weldment. The weld interpass temperatures were maintained at 20–110°C.

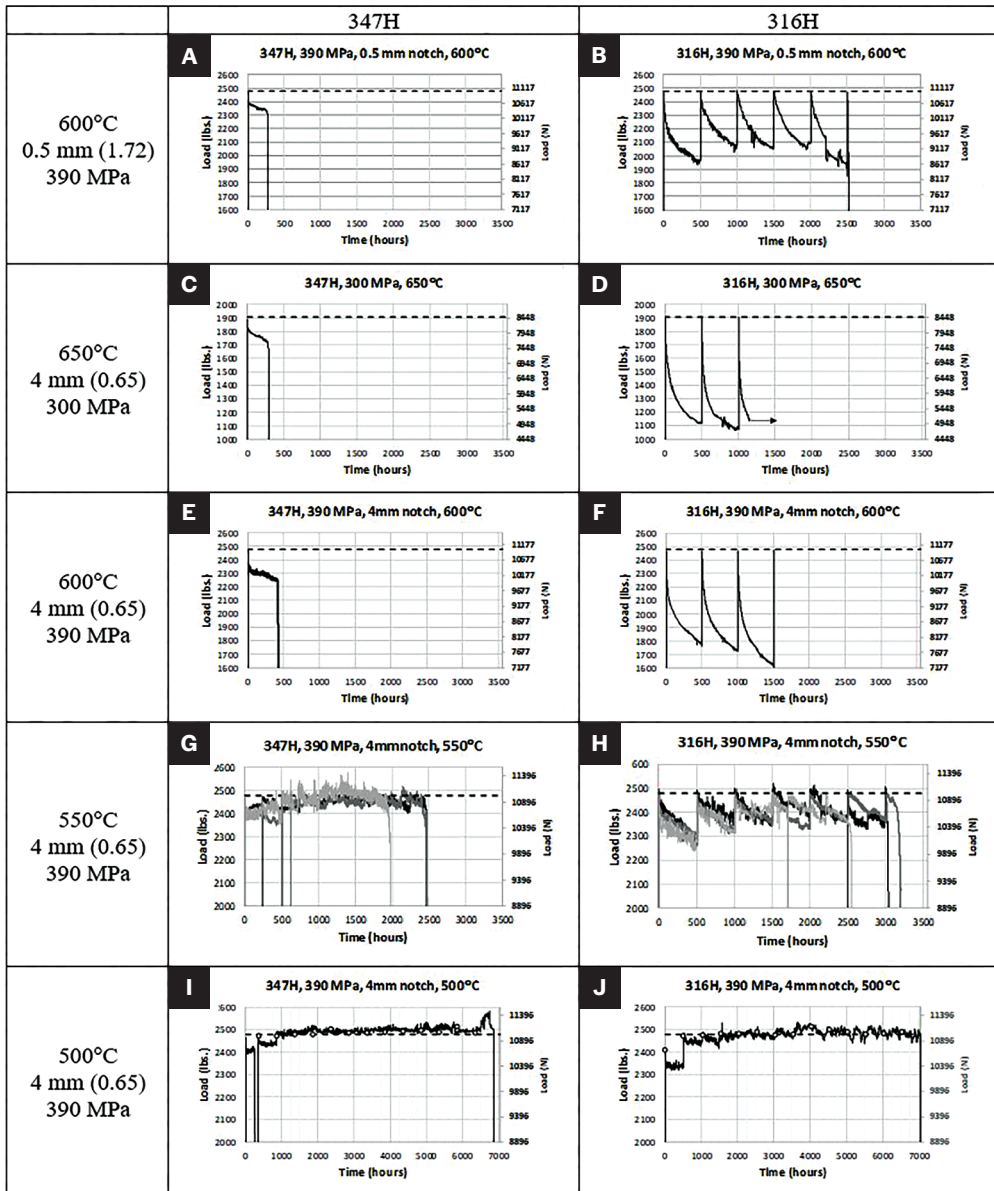


Fig. 4 – Comparison of load vs. time relaxation behavior for 347H (left column) and 316H (right column) as a function of test temperature and triaxiality. For the 500°C plots, the reloading time is indicated by the gray circles. The 347H showed more susceptibility (fewer cycles to failure) than the 316H except at 500°C, where neither sample failed in 14 cycles.

In austenitic stainless steels and specifically in 316H, the weld heat-affected zone (HAZ) is a location of concern for stress relaxation cracking (Ref. 51). A typical narrow groove weld macrograph is shown in Fig. 3A, and the location of the Bridgman-type notched tensile samples (Ref. 52) is shown in Fig. 3B. Hardness maps of as-welded 316H and 347H are given in Figs. 3C and D, with the weld fusion region spanning from -0.3 in. to $+0.3$ in. As indicated, the notch centers were taken in a region of increased hardness ($+0.157$ in. from the weld fusion line), with HRB values of ~ 89 – 91 , as compared to the base metal value of 80 HRB. The tensile samples were 6 in. long with a 0.236 in. diameter across the notch root.

These tests followed the work of Spindler and Smith, who used similar notched tensile bars and test param-

eters (e.g., 390 MPa net section stress at 550°C) to assess the effects of triaxiality and temperature on susceptibility of 316H stress relaxation cracking (Ref. 14). The matrix of test conditions assessed in this study is given in Table 5. As shown, four temperatures (500, 550, 600, and 650°C) and two notch radii (0.157 in. [4 mm] and 0.020 in. [0.5 mm]) were assessed for each of the two materials. These notch radii corresponded to ratios of mean stress (σ_m) to effective stress ($\bar{\sigma}$) (i.e., triaxiality values of 0.65 for the 4-mm notch and 1.72 for the 0.5-mm notch per Equation 2, where $d/2$ is the specimen diameter at the notch and R is the notch root radius) (Ref. 53). One sample per condition was tested, except for the 550°C and 0.65 triaxiality condition, where three tests were performed to better assess the variability of this method.

Table 5 – Summary of Stress Relaxation Cracking Tests Performed in This Study

Materials	Condition	Test Temperature (°C)	Notch Radius (Stress Triaxiality, σ_m/σ_e *)	
			4 mm (0.65)	0.5 mm (1.72)
			# of Tests Conducted	
Alloy 316H Welded with 16-8-2 Filler	316H HAZ from Gas Tungsten Arc Weldment	500	1	—
		550	3	—
		600	1	1
		650	1	—
Alloy 347H Welded with 16-8-2 Filler	347 HAZ from Gas Tungsten Arc Weldment	500	1	—
		550	3	—
		600	1	1
		650	1	—

*Defined as the ratio of the mean stress over the effective stress, where $\sigma_m/\sigma_e = 0.33$ represents uniaxial tension and $\sigma_m/\sigma_e = 2.5$ is equivalent to a sharp notch.

$$\text{Triaxiality} = \left(\frac{\sigma_m}{\bar{\sigma}}\right)_{max} = \frac{1}{3} + \ln\left(\frac{d}{2R} + 1\right) \quad (2)$$

For each test, the sample was brought to the test temperature, homogenized for a minimum of 1 h, and then loaded to the target net section stress (390 MPa or 300 MPa for the 650°C tests). The initial loading was performed in stroke control, and once the target load was reached, the sample was held at constant stroke for 500 h (21 days), which allowed stresses to relax and creep damage to accumulate. Of note, the servo-electric test frames used were capable of highly accurate control with a position resolution of 1.9×10^{-6} inches (Ref. 54). After the 500-h hold, the sample was reloaded to the target net section stress and again held in stroke control for 500 h. These cycles were repeated until either failure or 14 cycles were completed (7000 h under stroke control). Post-test, the samples were characterized for fracture mode via light optical and scanning electron microscopy. One complication in this testing procedure was that the applied load at constant displacement was influenced by changes in room temperature, which was responsible for overloading certain test cycles as well as for periodic 24-h variation in the load vs. time data. Future work will seek to minimize these concerns by better controlling room temperature to better than $\pm 2.5^\circ\text{C}$.

Results

Stress Relaxation Data

The load-time relaxation curves for these tests are given in Fig. 4, which compares the response of 347H to 316H. The top plots (4A and B) are a 1:1 comparison between the two alloys with a sharp notch (0.5 mm radius and a triaxiality of 1.72) at 600°C. As shown, the 347H sample failed in less than one cycle (during the first stroke hold) with limited stress relaxation, while the 316H sample lasted over five cycles with appreciable stress relaxation each cycle. Here, a cycle is defined as the accumulated time from the start of the first stroke hold, divided by 500 h (e.g., a test failing exactly at 500 h would have undergone one cycle). The remaining four plots (4C–J) compare the alloys as a function of temperature with a triaxiality of 0.65 (4-mm notch). Note that for the highest temperature test (650°C, plots 4C and D), the net section stress was reduced to 300 MPa vs. 390 MPa for the other tests.

At the 0.65 triaxiality and 650°C condition, the 347H sample (4C) again failed in less than one cycle, while the 316H test (4D) showed more resistance (3.1 cycles before being inadvertently overloaded). At 600°C (4E and F), both alloys showed appreciable stress relaxation (corresponding to a load decrease > 100 lb), though with 316H shedding significantly more load than 347H. The 347H sample again failed in less than one cycle, while the 316H sample survived for 3.20 cycles. At 550°C (4G and H), the 316H sample still

showed clear, though limited, stress relaxation (~ 200 lb) while the 347H showed no obvious relaxation. At 550°C, the 347H (4G) showed failures at 3.99 (Note: The sample that failed at 3.99 cycles was inadvertently held at 99% of the UTS [98% planned] for approximately two cycles, which may have contributed to early failure), 4.96, and 4.98 cycles,

while the 316H (4H) showed longer life with failures at 5.12 (Note: This sample failed just after the sixth reloading cycle. However, due to unplanned computer outages, the time under load was 2558 h), 6.07, and 6.40 cycles. At 500°C (4I and J), neither alloy showed appreciable load shedding nor failed within 14 500-h cycles.

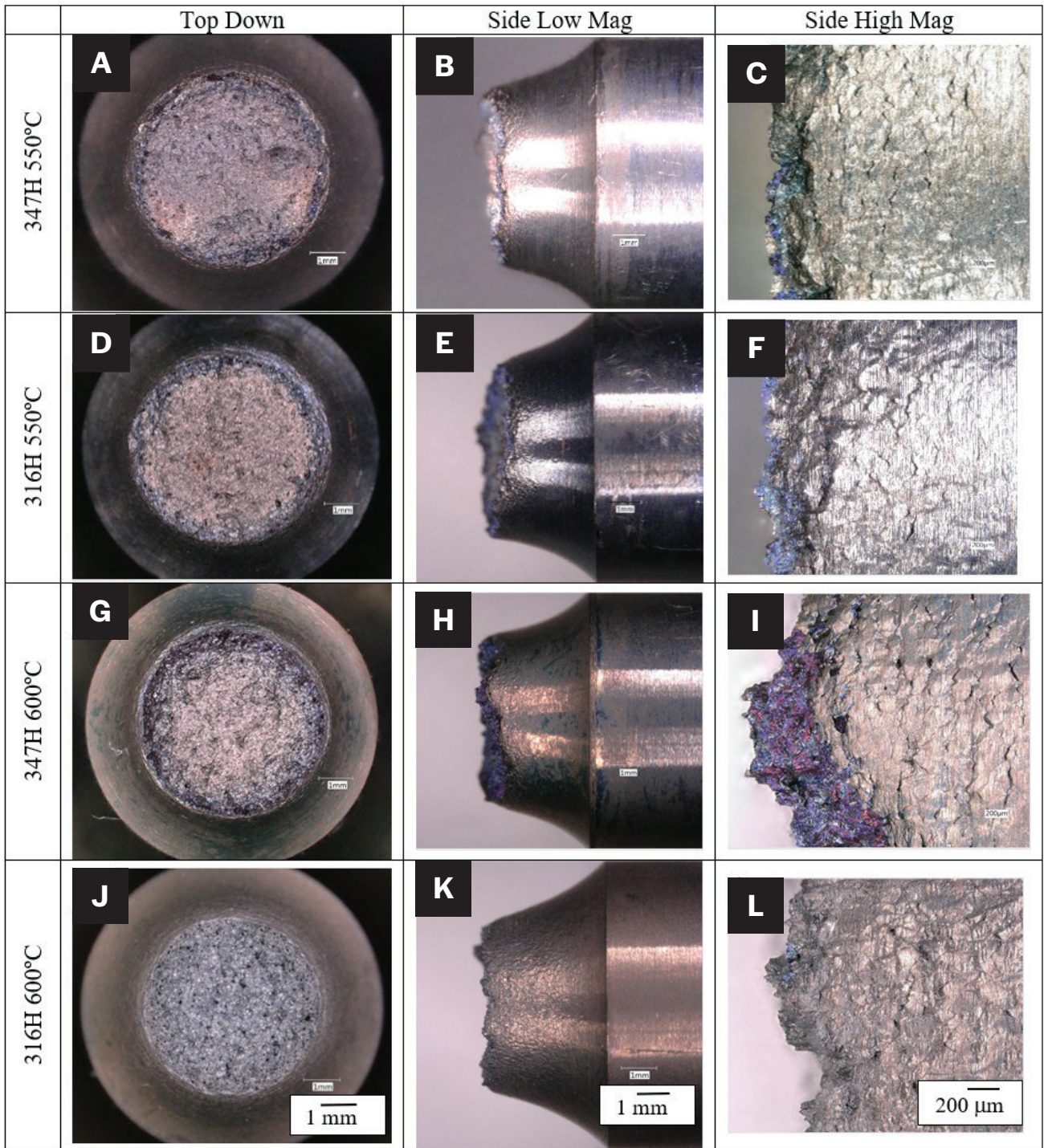


Fig. 5 – Low magnification optical fractography of the 347H and 316H samples with a triaxiality of 0.65 (4-mm notch).

Fractography

Light optical fractography of the failed 4-mm notched (triaxiality = 0.65) samples is given in Fig. 5. In Fig. 5, the 347H (Figs. 5A–C) and 316H (Figs. 5D–F) samples at 550°C, as well as the 347H sample (Figs. 5G–I) at 600°C, show a blue-tinted oxidized ring that is not present in the 316H 600°C test (Figs. 5J–L). Depending on the sample and temperature, the oxidized

ring was ordered at 0.2–0.5 mm. In the side magnification images, secondary intergranular cracking is evident along the notch in all the samples except for the 316H 600°C sample, where surface damage appears to be more like microvoids than intergranular cracks. At this time, the exact sequence of cracking is unclear, but it may be that the outer ring cracked first and the blue tint is from oxidation at 550°C.

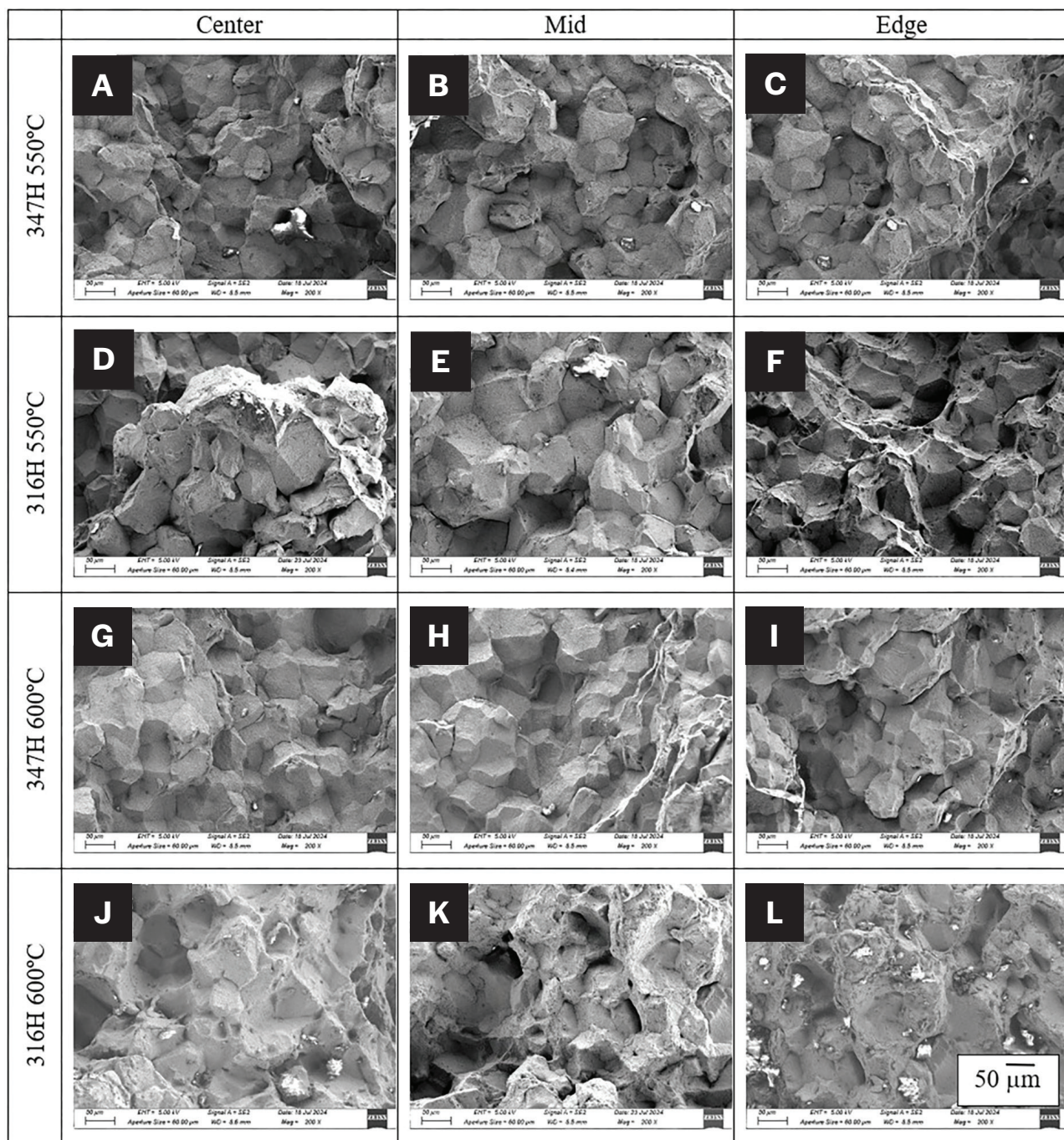


Fig. 6 – Low magnification fracture mode comparison of the 347H and 316H HAZ samples tested at 550°C and 600°C with a triaxiality of 0.65 (4-mm notch radii). Note the significant change in the 316H fracture mode between 550°C (brittle, intergranular) and 600°C (microvoids covering intergranular-sized features), while 347H displayed predominantly brittle intergranular cracking at both temperatures.

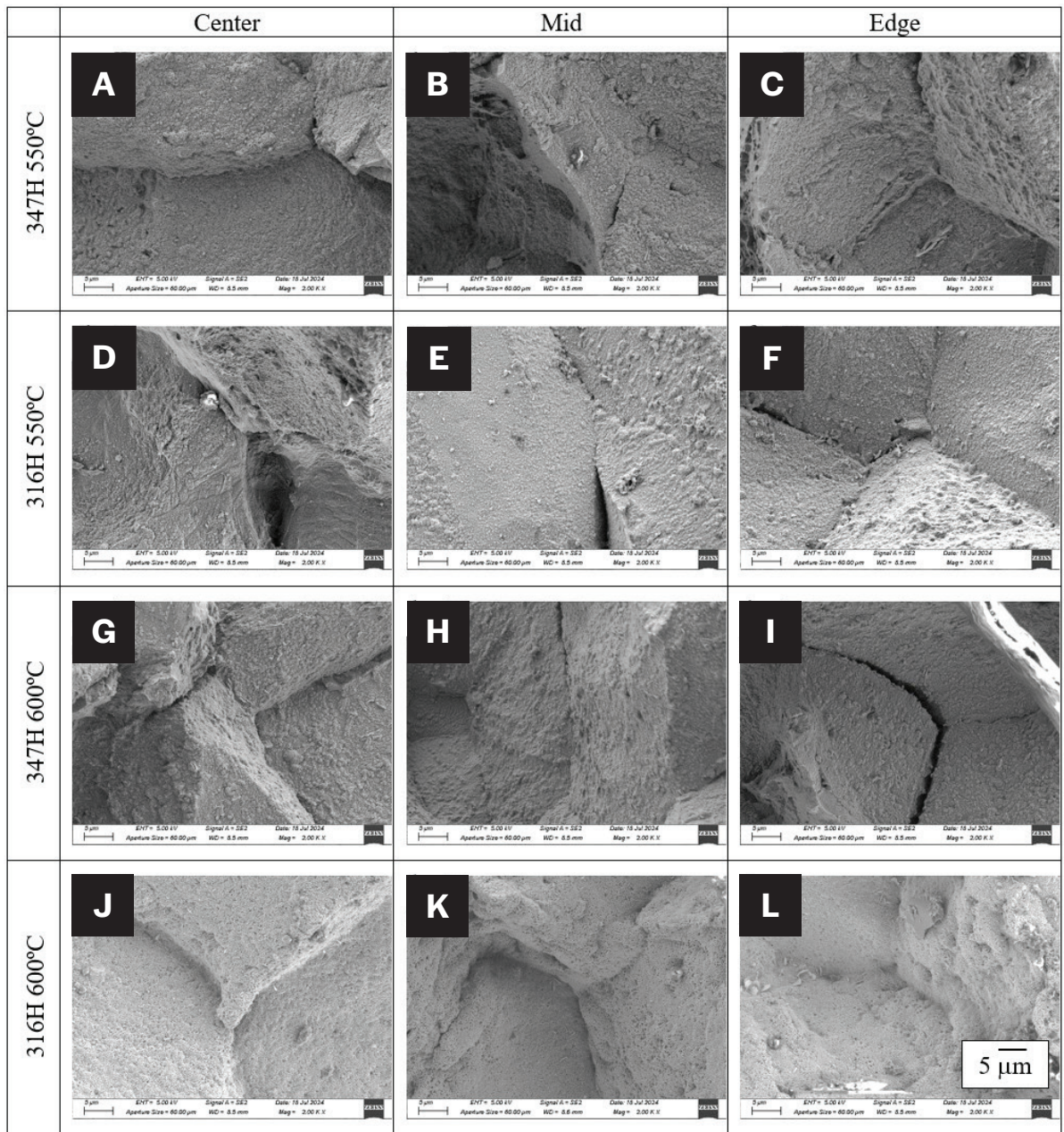


Fig. 7 – Higher magnification fracture mode comparison of 347H and 316H HAZ samples tested at 550°C and 600°C with a triaxiality of 0.65 (4-mm notch radii). Note the significant change in the 316H fracture mode between 550°C (brittle, intergranular) and 600°C (microvoids covering intergranular-sized features), while 347H displayed predominantly brittle intergranular cracking at both temperatures.

Scanning electron microscope (SEM) images are given in Fig. 6 (200X) and Fig. 7 (2000X). At 550°C, both alloys show a large extent of intergranular cracking, although the 316H sample does exhibit some microvoids (dark round features) in the center and mid-fracture surface locations. Both alloys exhibit ~ 200–300 microns of blue-tinted oxidized ring near the notch. At 600°C, the fracture modes of 347H and 316H diverge, consistent with the longer failure time of 316H. Here, 347H again shows ~ 100% intergranular cracking and deeper oxidation of ~ 500–700 microns from the notch surface. In contrast, the 316H sample is more ductile and does not

show the oxidized ring. The fracture mode in the 316H 600°C sample shows a fundamental change with fine (<< 1 mm in diameter) microvoids covering intergranular features. This change in fracture mode from brittle intergranular (347H at 600°C) to more ductile fracture (316H at 600°C) is highlighted in the SEM comparison of Fig. 8.

Additional light optical microscopy for the 600°C, 0.5-mm notch (triaxiality = 1.72) 347H/316H samples and the completed 650°C, 4-mm notch (triaxiality = 0.65), 347H sample is given in Fig. 9, with the corresponding scanning electron microscopy shown in Figs. 10 and 11. For the 600°C, 0.5-mm

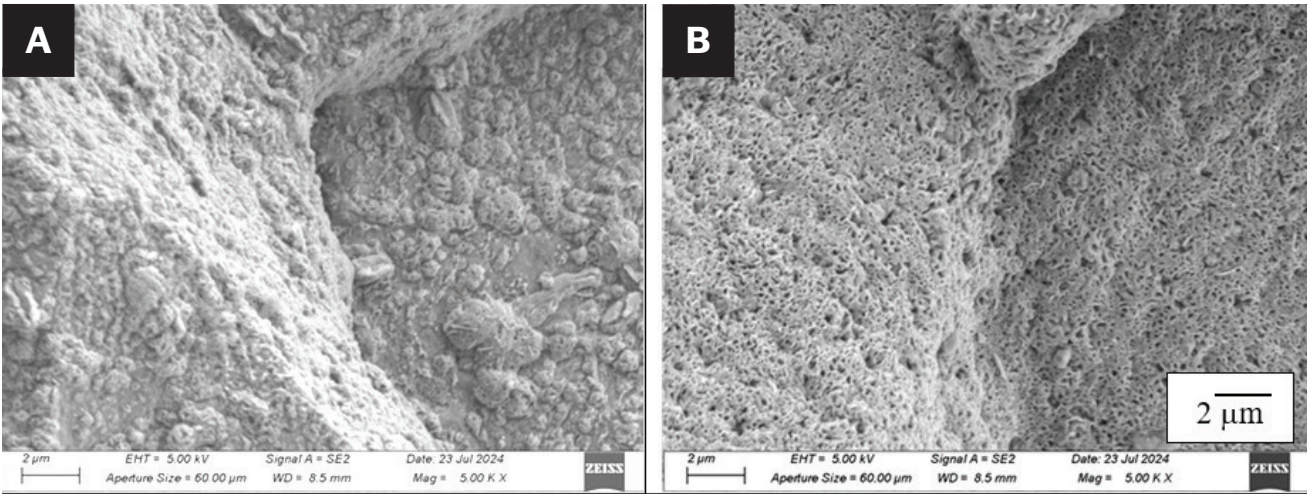


Fig. 8 – Illustration of the change fracture mode differences between 347H (left) and 316H (right). Note the extensive microvoid formation in the 316H sample, while the 347H displayed a more brittle, intergranular fracture. Tests were at 600°C, triaxiality = 0.65, and net section stress = 390 MPa.

Table 6 – Comparison of the Alloy’s Uniaxial Ultimate Tensile Strength and the Fraction of the UTS These Tests Were Conducted at

Test Temperature		500°C	550°C	600°C	650°C
Target Net Section Stress (MPa)		390	390	390	300
347H	UTS (MPa)	443	424	398	364
	Fraction of UTS	0.88	0.92	0.98	0.82
316H	UTS (MPa)	470	435	388	332
	Fraction of UTS	0.83	0.90	1.00	0.90

notch tests, the 316H sample shows a cup/cone type fracture, while the 347H sample is macroscopically flat. The SEM images show that the near-edge of the 316H sample displays intergranular cracking, but the bulk of the sample (the cup/cone region) is much more ductile and is a mix of shear and microvoids. In contrast, the 347H sample displays predominantly intergranular cracking (albeit with fine microvoids on the intergranular features in the bulk of the sample, the gray region of the fracture surface). In this 347H sample, we note the blue oxidized region on about 25% of the fracture surface (see the “Fracture Surface” images in Fig. 9), again indicating a different time of exposure to high-temperature air. Subsequent electron microscopy (Figs. 10 and 11) showed that the blue-tinted region failed in a ductile manner with significant microvoiding.

Discussion

Loading Conditions

While the alloys were compared at constant stress (390 or 300 MPa, depending on the test temperature), a better metric may be the applied stress relative to the alloy’s yield strength or ultimate tensile strength (UTS) at temperature. To illustrate this, ultimate tensile strength data for 347H were taken from the open literature (Ref. 55) and 316H data from separate testing at Kairos Power, and the test stress relative to the UTS was estimated in Table 6. As shown, the mechanical test conditions for each alloy were roughly equivalent over the four temperatures tested, with slightly higher fractional loading given to the 347H specimens at 500°C (0.88_{347H} vs. 0.83_{316H}) and 550°C (0.92_{347H} vs. 0.90_{316H}) and the 316H samples at 600°C (1.00_{316H} vs. 0.98_{347H}) and 650°C (0.90_{316H} vs. 0.82_{347H}). In future testing, using the fraction of the UTS will likely be a useful metric to better compare the reheat-type cracking resistance of different alloys and/or conditions of the same alloy.

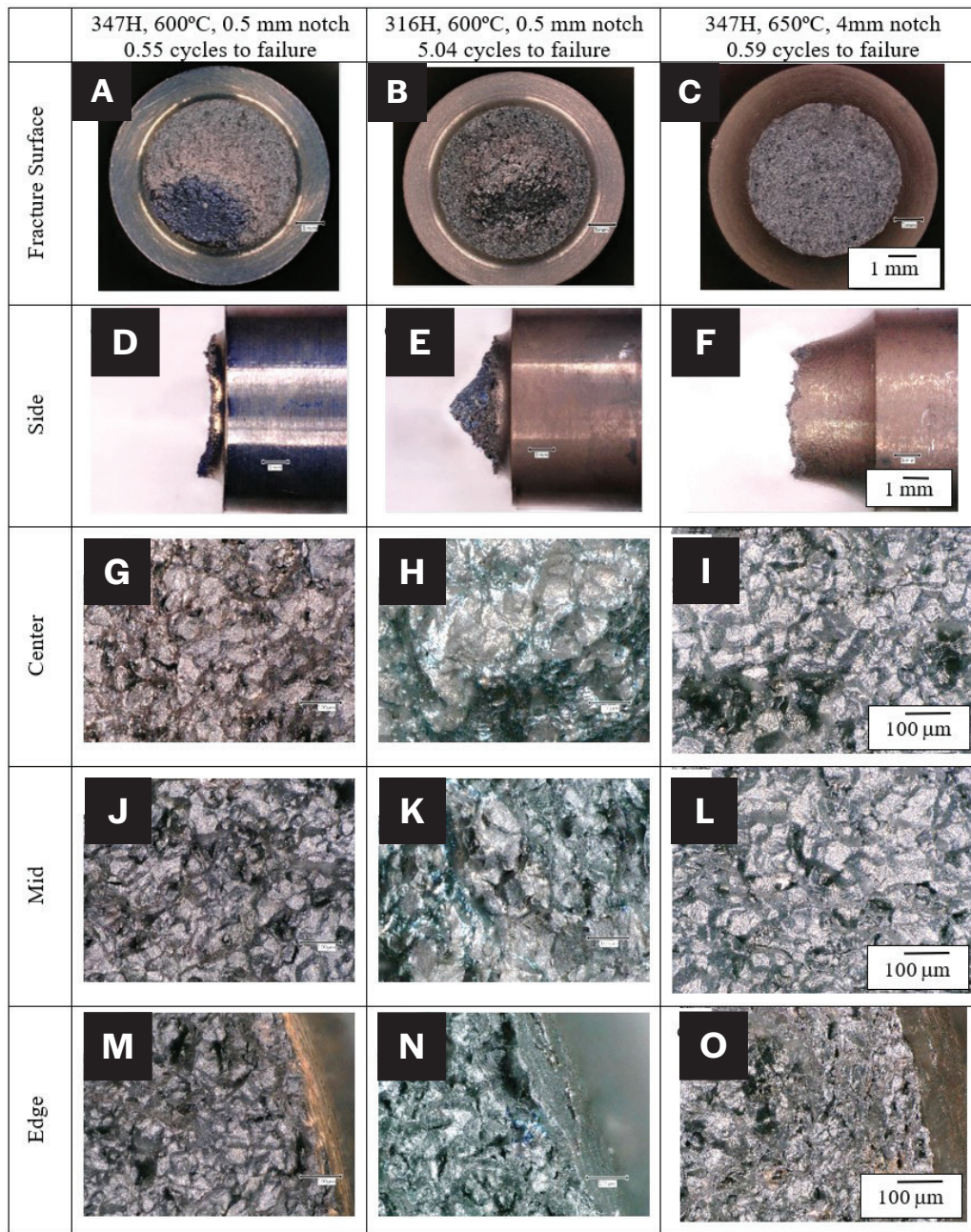


Fig. 9 – Comparison of 316H and 347H fractography at 600°C and at a triaxiality of 1.72 (0.5-mm notch) and 347H at 650°C and a triaxiality of 0.65. At 600°C, the 316H exhibited a more-ductile cup/cone type fracture and less intergranular cracking than the 347H sample.

Alloy	Cycles to Failure	Average	Standard Deviation
316H	5.12*, 6.07, 6.40	5.86	0.66
347H	3.99**, 4.96, 4.98	4.65	0.56

*This sample saw two unintentional unloadings due to test stand communication issues.
 **This sample was overloaded to 99% of the UTS for ~ 1000 h, which may have contributed to its shorter failure.

Validation of the Test Method

To better understand the accuracy of this test method, three replicate tests (triaxiality of 0.65, 4 mm radius notch) were conducted at 550°C for each alloy. Both alloys were loaded to a target net section stress of 390 MPa, corresponding to 0.92 of the uniaxial UTS for 347H and 0.90 for 316H, as shown in Table 6. These tests resulted in cycles to failure of 6.06, 6.20, and 6.60 for the 316H and 4.01, 4.98, and 5.04

for the 347H, as summarized in Table 7. In Table 7, note that one 316H sample (with a relatively short failure time of 5.12 cycles) suffered from two unintentional unloadings due to test stand communication issues. One 347H sample (with a relatively short failure time of 3.99 cycles) was mistakenly overloaded to ~ 397 MPa (or 0.99 of the UTS) vs. the target 390 MPa for ~ 1000 h of the test. Despite these complications, at 550°C, the two alloys appeared to show significantly different average numbers of cycles to failure (5.86 cycles ± 0.66 for 316H vs. 4.65 cycles ± 0.56 for 347H).

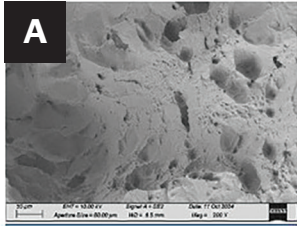
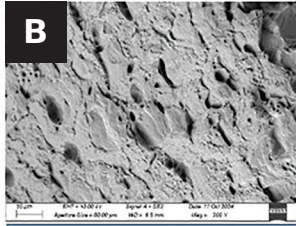
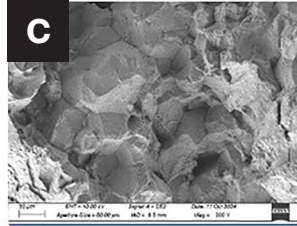
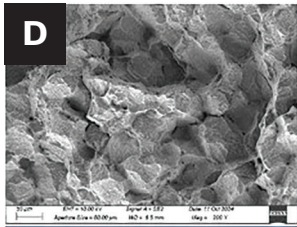
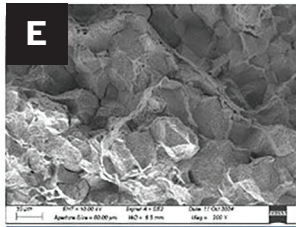
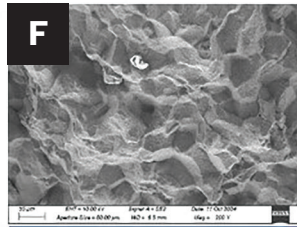
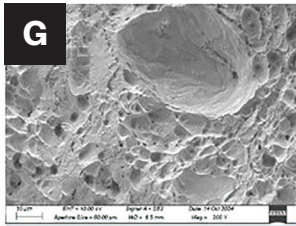
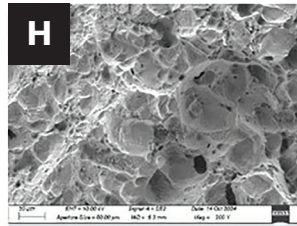
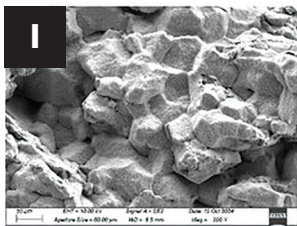
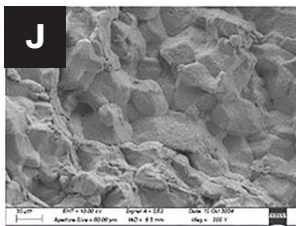
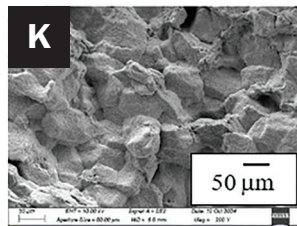
200X Magnification			
	Center	Mid	Edge
316H, 600°C, 0.5 mm notch 5.04 cycles to failure			
347H, 600°C, 0.5 mm notch 0.55 cycles to failure			
	Blue Oxidized Region		
347H, 650°C, 4mm notch 0.59 cycles to failure			

Fig. 10 – Low magnification SEM fractography of 316H and 347H at 600°C and at a triaxiality of 1.72 (0.5-mm notch) and 347H at 650°C and a triaxiality of 0.65.

Also of note is the metallurgical validation of the test method, with 347H and 316H producing intergranular cracking at 550°C, consistent with cracking in welded components (Refs. 2, 14, 56). Thus, cyclic notched bar stress relaxation tests were confirmed to be an accurate test method to produce stress relaxation cracking in a metallurgically relevant time/temperature regime and enable more-quantitative comparisons between alloys and the effects of temperature and stress state.

Fractography

The key findings from light optical and electron microscopy presented in Figs. 5–11 are summarized in Table 8. Note that in this table, the % reduction in area is not reported as the samples did not typically fail at the minimum diameter, and determination of the initial diameter at the failure plane was difficult to reconstruct, confounding this common estimate of ductility. Macroscopically, all the samples investigated except

Table 8 — Comparison of Stress Relaxation Test Performance and Fracture Modes; Key Differences Between the Two Alloys are Highlighted in Bold Text

Notch Radius		4 mm						0.5 mm			
Triaxiality		0.65						1.72			
Alloy HAZ	347H	316H	347H	316H	347H	316H	347H	316H	347H	316H	
Temperature	500°C		550°C		600°C		650°C		600°C		
Net Section Stress (MPa)	390	390	390	390	390	390	300	300	390	390	
Fraction of Uniaxial UTS	0.88	0.83	0.92	0.90	0.98–0.99	1.00	0.82	0.90	0.98	1.00	
Number of 500-h Cycles to Failure	> 14	> 14	3.99, 4.96, 4.98	5.12, 6.07, 6.40	0.85	3.20	0.59	> 3.12**	0.55	5.04	
Macroscopic Fracture			Flat	Flat	Flat	Flat	Flat			Flat	Cup/ Cone
Near Notch Fracture Surface Oxidized			Yes	Yes	Yes	No	No			Yes, but one side	No
Degree of IG Secondary Cracking			High	High	High	Low	Low	Test in-progress	Med.	Med.	
Degree of IG Fracture Notch			High	High	High	Fine voids on IG features	Fine voids on IG features		Fine voids on IG*	High	
Degree of IG Fracture – Midway			High	High	High				High*	No IG but micro-voids and shear	
Degree of IG Fracture - Center			High	High	High	High	High				

*Blue oxidized area is ductile microvoiding.

**This test was inadvertently overloaded at 3.12 cycles but did not fail.

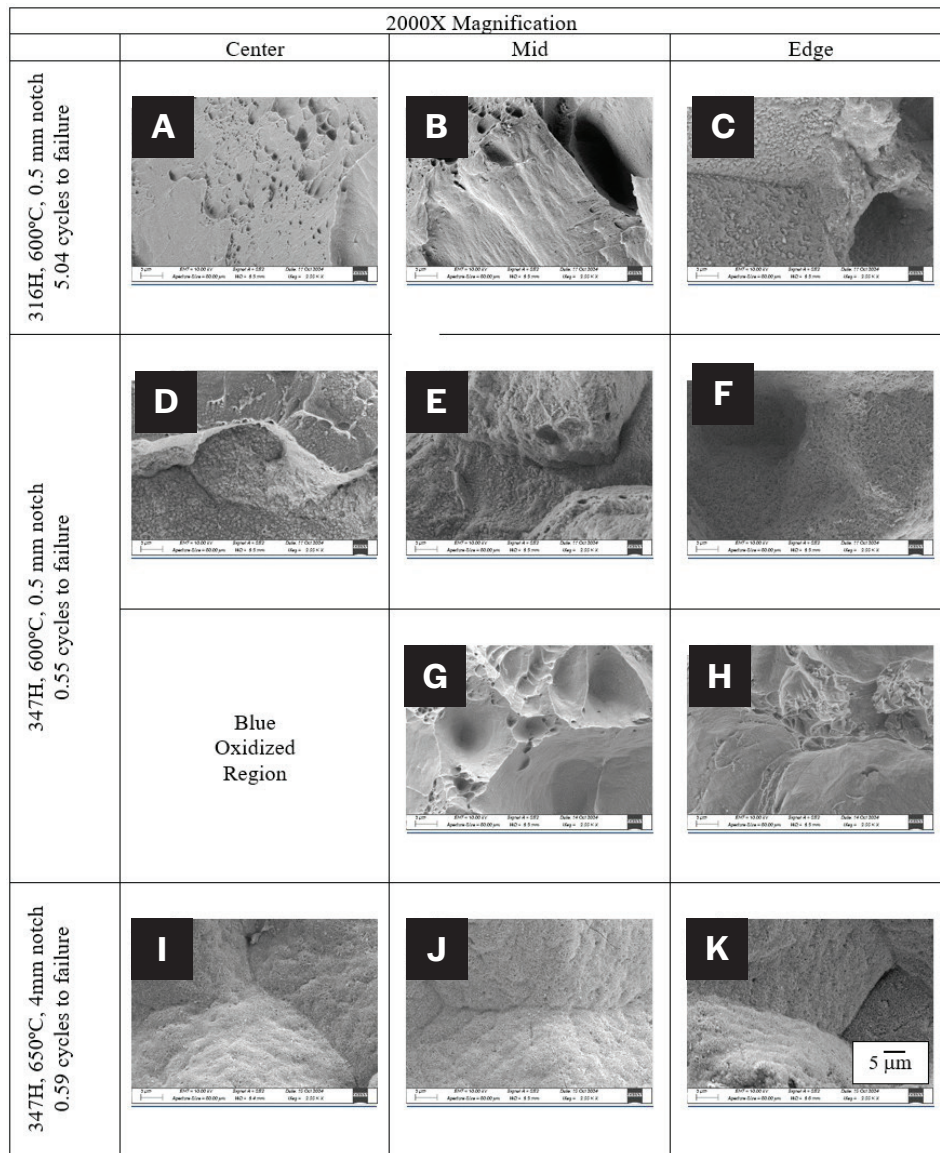


Fig. 11 – High magnification SEM fractography of 316H and 347H at 600°C and at a triaxiality of 1.72 (0.5-mm notch) and 347H at 650°C and a triaxiality of 0.65.

for 316H at 600°C (0.5-mm notch) displayed a flat fracture surface. The 316H sample at 600°C was notably a cup/cone-type fracture, indicative of the increased ductility in 316H at this temperature. Also of note is the presence of a distinctly oxidized near-surface layer in many that display intergranular fracture. This oxidized layer (the blue-tinged region of the fracture surface) was 300–500 microns in depth for the 347H samples at 550°C and 600°C. However, the 316H samples only display this oxidized region in the one sample susceptible to reheat-type cracking (550°C). The potential role of grain boundary oxidation on reheat-type cracking is unclear, but we note that other researchers have associated grain boundary oxide films (and sometimes a metallic filament encased in oxide) with reheat cracks (Refs. 3, 4). Somewhat anomalously, we also note that the oxidized region on 25% of the 347H, 600°C, 0.5-mm notch (triaxiality = 1.72) sample showed a ductile fracture in the oxidized region (~ 25% of the fracture

surface) and much more brittle intergranular fracture on the rest of the sample. This may have been a remaining ligament that failed in a ductile manner after significant intergranular cracking had occurred.

The fracture modes of the samples are more clearly illustrated in the SEM images. At 550°C (390 MPa and triaxiality = 0.65), both alloys were susceptible to reheat-type cracking (i.e., susceptible to brittle intergranular failure, which was exacerbated by triaxial stresses), and the fracture mode was predominantly intergranular. As the temperature increased to 600°C, there were significant differences in the fracture mode, with 347H displaying predominantly intergranular failure but 316H showing significantly more ductility. While intergranular features were still evident in the 316H sample, the facets were completely covered by fine microvoids, as shown in Fig. 7 and highlighted in Fig. 8. At 650°C, the 347H sample continued to display susceptibility to reheat-type

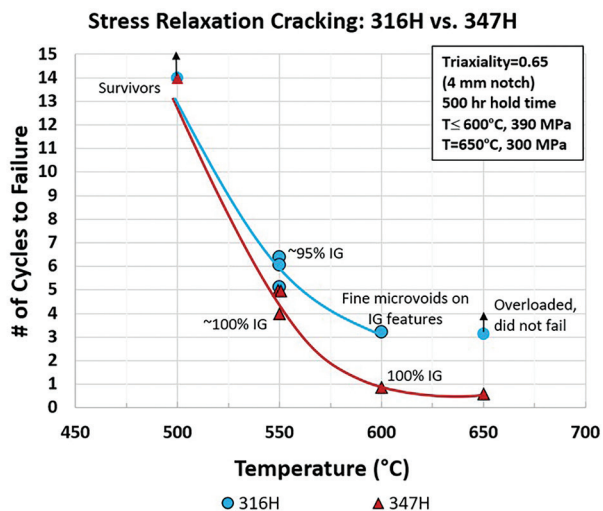


Fig. 12 — Summary of the 0.65 triaxiality (4-mm notch) stress relaxation cracking tests showing that 316H displayed significantly more resistance than 347H. Additionally, the change in fracture mode of 316H at ~600°C was a significant difference relative to 347H, which still displayed 100% intergranular fracture and short failure times at 600°C and 650°C.

cracking with a short failure time (0.59 cycles) and intergranular-type cracking, albeit with some increase ductility as microvoids covered most of the intergranular fracture features. The corresponding 650°C, 316H, 0.5-mm notch (triaxiality = 0.65) test was inadvertently overloaded at 3.12 cycles but did not fail, indicating significantly more resistance to reheat-type cracking.

Effect of Temperature: 347H vs. 316H

A major goal of this study was to quantitatively assess the susceptibility of 316H HAZ material relative to an alloy of known susceptibility (347H HAZ). Comparative tests at one triaxiality (0.65 or 4 mm radius notch) as a function of temperature are shown in Fig. 12. As shown, both alloys showed resistance at 500°C with no failure after 14 x 500-h cycles. However, at 550°C, stress relaxation cracking was triggered in both alloys, but 316H (5.86 average cycles to failure) showed more resistance than 347H (4.65 average cycles to failure). In each alloy at 550°C, the fracture mode was essentially 100% intergranular fracture. At 600°C, the susceptibility of the two alloys continued to diverge, with 316H failing in ~3.20 cycles and 347H failing in 0.85 cycles. Notably, the fracture mode in 316H at 600°C changed to a more-ductile fracture with fine microvoids covering intergranular-sized features. In contrast, the fracture mode of 347H at 600°C remained brittle, with intergranular failure. Lastly, tests at 650°C continued to support this different behavior between the two alloys, with 347H again failing in greater than one cycle (0.59 cycles), while the 316H test survived 3.12 cycles before being accidentally overloaded. Note that the 650°C tests were conducted at 300 MPa (vs. 390 MPa for the lower temperature tests).

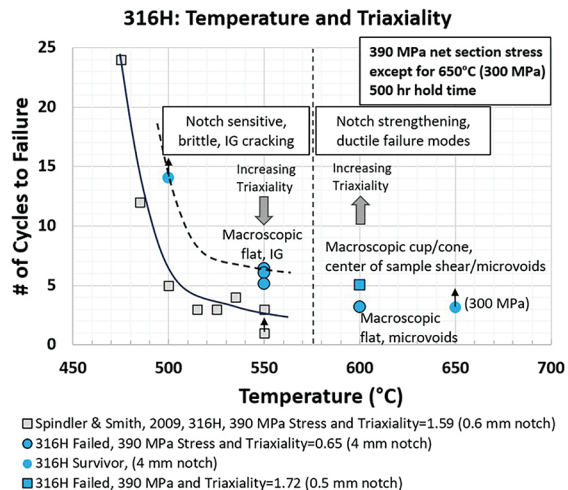


Fig. 13 — Summary of the effects of temperature and triaxiality on the cracking resistance of 316H heat-affected zones. At temperatures between 475°C and 550°C, the susceptibility of the 316H HAZ samples increased with increasing temperature and triaxiality. However, at 600°C, the 316H displayed notch strengthening and a change to a more-ductile fracture mode, indicating resistance to reheat-type cracking.

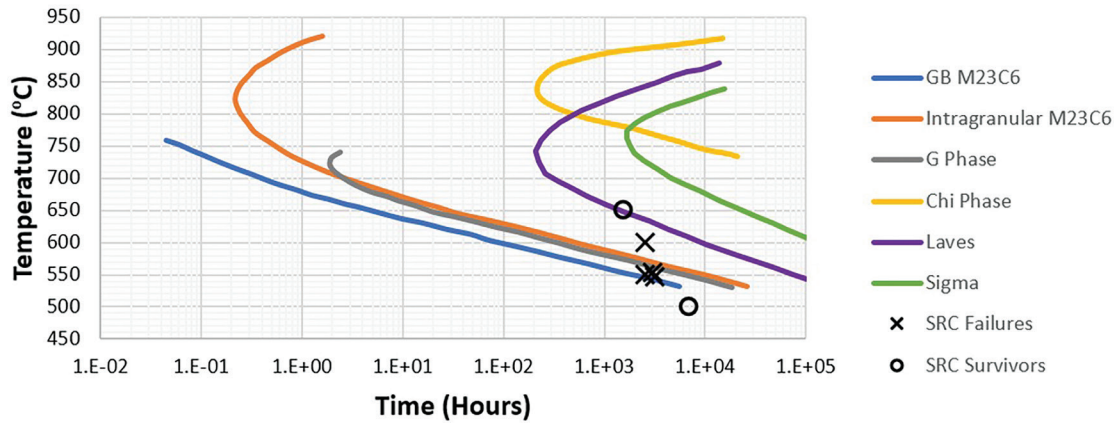
Effects of Temperature and Triaxiality on 316H

Literature data are plotted along with data from the present study in Fig. 13 to better understand the effects of test temperature and triaxiality. As shown by the data of Spindler and Smith (Ref. 14) for ex-service 316H HAZ specimens (gray squares), increasing temperature from 475°C to 550°C increases the susceptibility to reheat-type cracking in this material. This trend was confirmed by the present study (blue circles at 500°C and 550°C) using samples with lesser triaxiality (triaxiality = 0.65, 4 mm radius notch vs. triaxiality = 1.59, 0.6 mm radius notch for Spindler & Smith). We estimated the triaxiality per Equation 1, which differs from Spindler & Smith, who used finite element analyses. Furthermore, we note that the heat investigated by Spindler and Smith was notably higher in sulfur content (0.014 wt-% for cast 69431 vs. 0.003 wt-% in the current study) and was from 316H exposed to 490–520°C for up to 65,000 h prior to testing. Despite these differences, intergranular cracking was readily produced at lower triaxiality in the present work on as-received 316H. Future work will seek to conduct 1:1 experiments relative to the work of Spindler and Smith to better assess potential metallurgical factors.

However, at a test temperature of 600°C, this notch sensitivity appeared to reverse for 316H, with the higher triaxiality sample (triaxiality = 1.72) failing at a longer time (5.05 cycles) than the lower triaxiality sample (triaxiality = 0.65 at 3.20 cycles). This change in notch sensitivity was accompanied by a change in fracture mode from brittle intergranular cracking in 316H at 550°C to a significantly more-ductile fracture mode at 600°C (see dashed line in Fig. 13), with fine microvoids covering intergranular-sized features, as discussed previously and

A

316H TTT after NIMS



B

347H TTT after Powell and Sourmail

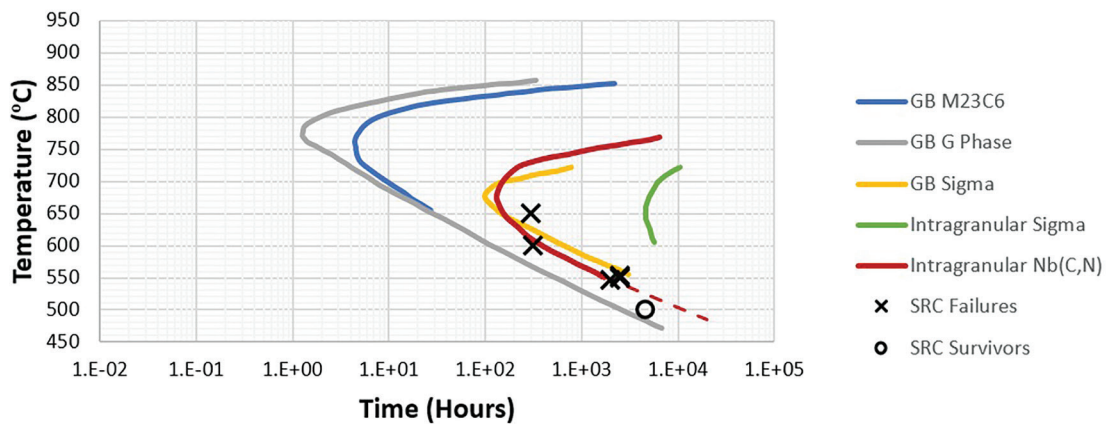


Fig. 14 – Comparison of time-temperature-transformation kinetics of: A – 316H (Refs. 61, 67); B – 347H (Refs. 59, 60) with stress relaxation cracking data from this study. The correlation of failure times/temperatures in 347H indicates the start of intragranular Nb(C,N) precipitation promotes cracking.

Table 9 – Summary of Theoretical Precipitation-Induced Strains

Phase	Orientation Relationship	Lattice Parameters	Interplanar Spacing, (nm)	% Misfit with $\gamma^* = (d_{ppt} - d_{\gamma}) / d_{ppt} \times 100$
FCC Matrix	—	$a_{\gamma} = 0.360 \text{ nm}$	$d_{\{100\}} = 0.360$ $d_{\{111\}} = 0.254$	—
FCC Nb(C,N)	$\{111\}_{\gamma} // \{111\}_{M(C,N)}$	$a_{NbC} = 0.447 \text{ nm}$ $a_{NbN} = 0.440 \text{ nm}$	$d_{\{111\}} = 0.316$ $d_{\{111\}} = 0.311$	+20% +18%
FCC TiC	$\{111\}_{\gamma} // \{111\}_{M(C,N)}$	$a_{TiC} = 0.433 \text{ nm}$ $a_{TiN} = 0.424 \text{ nm}$	$d_{\{111\}} = 0.306$ $d_{\{111\}} = 0.300$	+17% +15%
FCC $M_{23}C_6$	$\{100\}_{\gamma} // \{100\}_{M_{23}C_6}$	$a_{M_{23}C_6} = 1.057 \text{ nm to } 1.068 \text{ nm}$	(i.e., $a_{M_{23}C_6} \sim 3a_{\gamma}$) $d_{\{100\}} = 0.352$ $d_{\{100\}} = 0.356$	-1% -2%

*Note that substoichiometric MC-type precipitates likely have lesser misfit strains, ~ 5%, as discussed in Ref. 57.

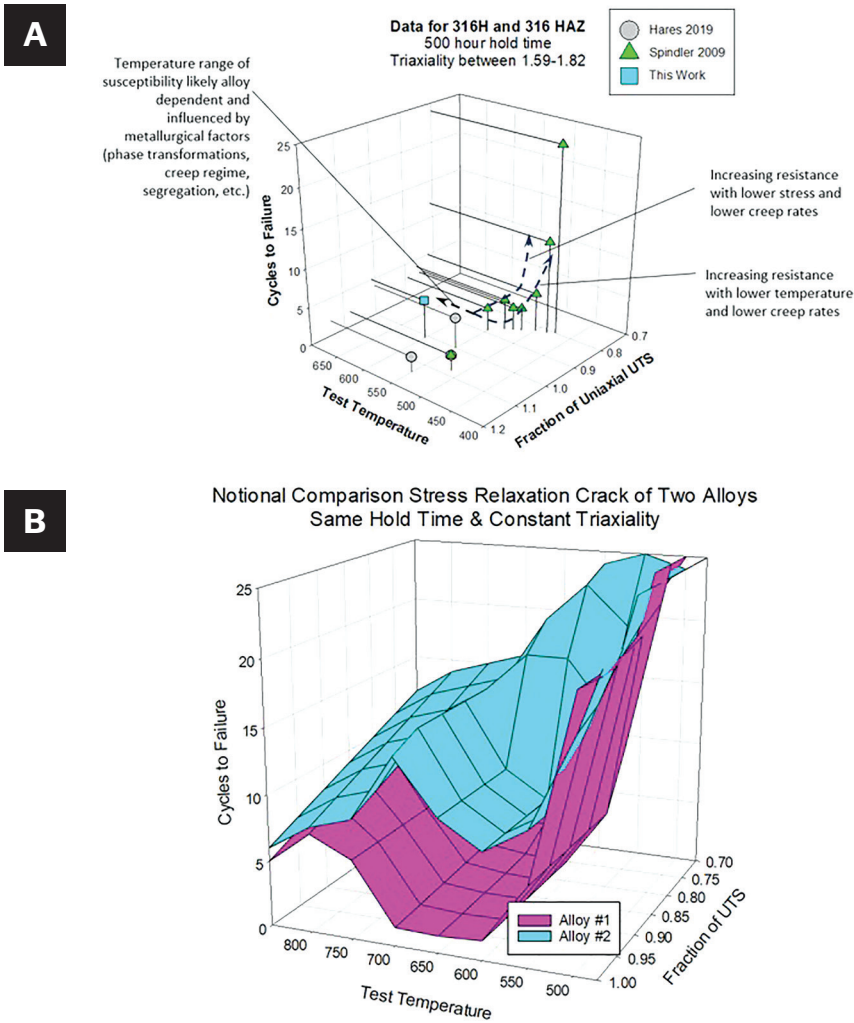


Fig. 15 — A — A data compilation for 316H stress relaxation cracking dependence, which suggests strong effects of applied stress and test temperature; B — illustration of how more-comprehensive data may enable reliable comparison of stress relaxation cracking susceptibility, where Alloy #1 shows significantly greater susceptibility to reheat-type cracking.

shown in Fig. 7. Based on these observations, 316H appeared to be developing resistance to reheat-type cracking (again, defined here as intergranular cracking which is exacerbated by triaxial stresses). The notion of resistance to reheat-type cracking in 316H at 600°C is consistent with Christoffel's notched bar 316H creep-rupture testing on 316H (Ref. 33), which showed notch strengthening in 316H at 593°C at times up to 10,000 h. In complementary research, Christoffel showed susceptibility to reheat-type cracking of 347 stainless steel at 593°C (Ref. 32). Note that a 316H test at 650°C and 300 MPa (90% of the UTS) is in progress to better confirm this recovery.

Metallurgical Differences between 347H and 316H

The results from this study demonstrate the increased susceptibility of 347H stainless steel heat-affected zones to reheat-type cracking relative to 316H. Several studies have

noted the susceptibility of the stabilized grades of austenitic stainless steel and associated it with precipitation hardening (Refs. 2, 4, 13, 33), which warrants a closer examination of the metallurgical changes in these alloys. To further this comparison, select orientation relationships, lattice parameters, and theoretical misfit strains for Nb(C,N), Ti(C,N), and $M_{23}C_6$ -type carbides are given in Table 9 (Refs. 57–59).

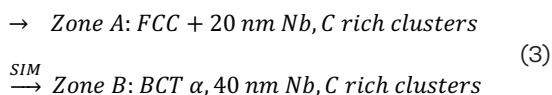
For the stabilized grades, Nb(C,N) precipitation in 347 and Ti(C,N) precipitation in 321 have theoretical misfit strains that are appreciable and positive (+15–20%), while chromium-rich $M_{23}C_6$ -type carbides have theoretical misfit strains that are relatively small and negative (–1–2%). As discussed by Andren (Refs. 57–58), MC-type carbides in 347 and 321 likely form sub-stoichiometrically, often on existing or geometrically necessary dislocations with ~ 5% misfit strain. This initial strain increases with aging as the composition moves toward 1:1 (Nb or Ti: C + N). Thus, for the stabilized grades, there is likely a precipitation-induced strain ~ 5%, which increases with time,

while for 316 (or 304) stainless steel, precipitation-induced strains are significantly smaller.

The stress relaxation failure times and temperatures for 347H and 316H are compared to the time-temperature-transformation (TTT) diagrams for each alloy in Fig. 14. These TTT diagrams are experimentally based and estimate the onset of each phase transition (Refs. 59–61). As shown, the 316H failures (top plot) have some correlation with the onset of grain boundary M₂₃C₆-type carbide precipitation at 550°C but not at 600°C or 650°C. However, the 347H failures are correlated with the precipitation of intragranular Nb(C, N) in the range of 550–650°C. These observations, combined with the theoretical misfit strains in Table 9, indicate that precipitation-induced strains likely contribute to the cracking sensitivity of 347 and 321 stainless steels. The notion that Nb(C,N) precipitation produces precipitation-induced stresses and strains fits well with the observations of Li and Messler in their study of reheat cracking in 347 stainless steel (Ref. 13). In that work, cracking sensitivity showed a C-curve dependence (Note: The C-curve times reported by Li were likely biased toward shorter time as they did not account for the time to bring the test sample to temperature or any soak time; if that additional time were considered, the C-curve presented by Li would likely be more consistent with intragranular Nb(C,N) precipitation in the TTT diagram). Nb-rich phases were detected via energy dispersive spectroscopy on cracked samples, and constant load tests at temperature showed a volumetric contraction of the sample. Similarly, Yang correlated 347 failure times with C-curve kinetics that correspond to intragranular Nb(C, N) precipitation (Ref. 62).

More recently, Kim et al. discussed the susceptibility of 347H to reheat cracking with the strengthening that occurs due to precipitation of NbC (Ref. 63). Their detailed transmission electron microscopy analysis of the 347H HAZ indicates that NbC forms via a complex process where precipitation-induced stresses and strains occur, produce strain-induced martensite, and promote reheat cracking. Specifically:

Nb and C rich FCC γ in HAZ



\rightarrow FCC NbC, 20 – 50 nm precipitates with $a = 0.447 n$

noting that $\gamma(111)/\alpha(100)$ and $\gamma(200)/\alpha(101)$ coincide on the zone axis of $\gamma < 011 > // \alpha < 111 >$ and that the NbC phase likely precipitates in the α -BCC phase (which is likely strain-induced martensite). In the Author's view, both mechanisms (precipitation-induced stress-strain and hardening/loss of toughness) are important factors contributing to the known susceptibility of 347 stainless steel.

While grain boundary M₂₃C₆ precipitation has been shown to play a critical role in the DDC susceptibility of Ni-30Cr alloys (Refs. 10, 12), there is no clear evidence that either inter- or intragranular chromium carbide precipitation played a role in the susceptibility of 316H in the present work. In part, this was likely due to the lesser extent of precipitation in 316H than in A690, where carbon solubility is very low

and extensive grain boundary carbide precipitation occurs at very short times (Refs. 10, 12).

As shown in Fig. 14, the 316H failure times and temperatures did not generally correlate with any precipitation reaction. Still, they were likely controlled by the accumulation of grain boundary creep damage in this stress state/temperature regime, where grain boundary voids nucleate. Still, their growth may have been limited by slow bulk diffusion. There is extensive literature and active research into the mechanisms of this regime of reduced creep ductility and grain boundary fracture, and it provides additional background relevant to austenitic stainless steels (Refs. 64–66).

Suggestions for Future Work

Given that reheat-type cracking is a complex phenomenon that can be influenced by several mechanical factors (applied stress, triaxiality, elastic follow-up, etc.) and metallurgical factors (time at temperature, phase transformations, plastic strain, grain boundary metalloid segregation, etc.), the need for a standardized test method that relates to the time-temperature regime where actual components fail is of critical importance. When cracking occurs at timescales where both creep damage accumulation and metallurgical factors influence cracking (i.e., reheat cracking, strain-age cracking, and stress-relaxation cracking, as per Fig. 1), notched bar stress relaxation tests appear to be a reliable and accurate method of comparing cracking susceptibility.

To better understand susceptibility and make quantitative comparisons between alloys or of an alloy in different conditions, conducting systematic stress relaxation tests, such as an f (test temperature, net section stress) at constant triaxiality and hold time, is suggested as a best practice. Both literature data and the results from this work on 316H are compiled in Fig. 15 (top graph) to illustrate this. As shown, 316H is susceptible at $\sim 550^\circ\text{C}$ and as the net section stress approaches 90% of the UTS, but limited data show resistance at lower temperatures and with lower net section stress. Expanding on the differences between 316H and 347H shown in this study (see Fig. 12), a more useful comparison could be made with testing as a function of temperature and applied stress and relating these to the appropriate TTT diagram. This comparison is shown schematically in Fig. 15 (bottom), where the blue curve may represent the behavior of an alloy like 316H, where failure is largely driven by creep damage, and the pink curve represents a similar alloy but with increased susceptibility due to a deleterious phase transformation.

Conclusions

- Notched bar stress relaxation tests are a reliable and accurate method to assess reheat-type cracking where creep damage and metallurgical factors are of interest. The ability to precisely control the stress state, simulate the effect of elastic follow-up, and produce intergranular cracking at prototypical test times and temperatures are key advantages of this test method.

- Replicate tests performed at 550°C showed remarkable consistency, with 347H failing at 3.99 cycles, 4.96 cycles,

and 4.98 cycles and 316H failing at 5.12 cycles, 6.07 cycles, and 6.40 cycles. Improved test control (especially laboratory temperature control) is expected to further decrease test-to-test variability.

■ Notched bar testing showed that at equivalent triaxial stress state and temperature, 347H was more susceptible to cracking than 316H. While both alloys showed resistance to reheat cracking at 500°C (no failures in 14 cycles), 347H failed more quickly than 316H at 550°C (~ 4.65 vs. ~ 5.86 cycles) and 600°C (0.85 vs. 3.20 cycles). The divergent behavior at 600°C was notable, where 347H displayed nearly 100% brittle intergranular fracture but 316H showed significantly more ductility with fine microvoids covering intergranular-sized features. This trend continued at 650°C with 347H failing at 0.59 cycles while the 316H test survived > 3.12 cycles.

■ The 347H failure times and temperatures correlated well with the start of intragranular Nb(C,N) precipitation. Consistent with the work of Li and Messler (Ref. 13), this indicates a precipitation-induced stress or strain that contributes to cracking in 347H but not in 316H and helps explain the known susceptibility of the stabilized grades of austenitic stainless steel.

■ These findings illustrate the utility of using notched bar stress relaxation tests to better understand the key factors that control reheat-type cracking and to make quantitative comparisons between alloys and material conditions. Adopting a standard testing methodology would help enable 1:1 data comparison between researchers and facilitate both mechanistic understanding and the development of engineering solutions to mitigate stress relaxation cracking in components.

■ A compilation of literature data for 316H indicates strong dependencies on net section stress, test temperature, and triaxiality. Mapping out susceptibility to reheat cracking as a function of test temperature and a fraction of UTS tested vs. cycles to failure at a given triaxiality and hold time is suggested as important future work to compare the susceptibility of different conditions and/or different alloys to reheat-type cracking.

Acknowledgments

This research was guided by the significant developments in understanding stress relaxation/reheat cracking in austenitic stainless steels, starting with the contributions of Bob Christoffel at the General Electric Company in the 1960s as well as extensive work performed by or sponsored by British Energy and EDF Energy focused on advanced gas reactor issues. The authors thank Robert McReynolds, Dr. Mark Petkov, and Dr. Nam Nguyen at Kairos Power for their significant contributions to this research. Lastly, we wish to thank Dr. Gabriel Meric and Dr. Micah Hackett, who managed the execution of this work.

References

1. Picker, C., and Fraser, A. S. 1996. Experience of cracking in austenitic stainless components of the UK prototype fast reactor. *International Journal of Pressure Vessels and Piping* 65: 283–293.
2. Dhooge, A. 1996. Survey on reheat cracking in austenitic stainless steels and Ni base alloys. *Welding in the World* 41: 206–209.
3. van Wortel, J. C. 1998. “Relaxation cracking in the process industry, an underestimated problem.” In *Baltica IV: Plant Maintenance*

For Managing Life And Performance, edited by Hietanen, S., and Auerkari, P., 637–647. Helsinki, Finland: VTT.

4. van Wortel, H. 2007. Control of relaxation cracking in austenitic high temperature components. *CORROSION* 2007, 1-13.
5. Yoon, K. B., Yu, J. M., and Nguyen, T. S. 2015. Stress relaxation cracking in 304H stainless steel weld of a chemical reactor serviced at 560°C. *Engineering Failure Analysis* 56: 288–299.
6. Yu, Z., et al. 2020. Cracking risk mitigation in molten salt 347H SS hot tank welds. *ASES Solar Conference*.
7. Rensman, J. W., Spindler, M. W., and Shargay, C. 2023. Stress relaxation cracking, a misunderstood problem in the process industry. *Pressure Vessels & Piping Conference*, 1–11.
8. Pickle, T., et al. 2024. Stress relaxation cracking of alloys at temperatures higher than 540°C. *National Renewable Energy Lab*, 1–140.
9. Dhooge, A. 1987. Reheat cracking - A review of recent studies. *International Journal of Pressure Vessels and Piping* 27: 239–269.
10. Young, G. A., et al. 2008. The mechanism of ductility dip cracking in nickel-chromium alloys. *Welding Journal* 27(2): 31-s to 43-s.
11. van Wortel, H. 2009. Control of relaxation cracking in austenitic high temperature components. *VeMet Conference*, Marknesse, The Netherlands.
12. Young, G. A., et al. 2020. “Welds for nuclear systems.” In *Comprehensive Nuclear Materials*, edited by Konings, R. J. M., and Stoller, R. E., 517–544. Elsevier.
13. Li, L., and Messler, R. W. 2000. Stress relaxation study of HAZ reheat cracking in Type 347 stainless steel. *Welding Journal* 79(6): 137-s to 144-s.
14. Spindler, M. W., and Smith, M. C. 2009. The effect of multiaxial states of stress on creep failure of Type 316H under displacement control. *ASME 2009 Pressure Vessels and Piping Division Conference*, 1–7.
15. Hughes, W. P., and Berry, T. F. 1967. A study of strain-age cracking characteristics in welded Rene 41 - Phase I. *Welding Journal* 46: 361-s to 370-s.
16. Berry, T. F., and Hughes, W. P. 1969. A study of the strain-age cracking characteristics in welded Rene 41 - Phase II. *Welding Journal* 48: 505-s to 513-s.
17. Franklin, J. E., and Savage, W. F. 1974. Stress relaxation and strain-age cracking in Rene 41 weldments. *Welding Journal* 53(9): 380-s to 387-s.
18. Borland, J. C. 1960. Cracking tests for assessing weldability. *British Welding Journal* 7(10): 623–637.
19. Howard, R. D., and Gooch, T. G. 1972. Reheat cracking in austenitic stainless steels. *The Welding Institute Research Bulletin* 13(4): 112–115.
20. Howard, R. D., and Gooch, T. G. 1972. Reheat cracking in austenitic stainless steels Part 2. *The Welding Institute Research Bulletin* 13(5): 145–147.
21. Spindler, M. W. 2004. The use of Borland specimens to reproduce reheat cracking in Type 316H. *International Conference on High Temperature Plant Integrity and Life Extension*, 1–12.
22. Dennis, R. J., Easterbrook, L. E., and Leggatt, N. A. 2005. Application of modern weld modelling techniques in the design of a ring weld reheat cracking test specimen. *Pressure Vessels & Piping Conference*, 1–10.
23. Price, A., et al. 2009. Revised weld residual stress and creep damage assessments. *ASME 2009 Pressure Vessels and Piping Conference*, 1–10.
24. Berre, W. H., and Schmitz, M. J. 2019. Reheat cracking initiation assessment in nuclear plant stainless steel components at creep conditions. *SMIRT-25*, 1–10.

25. Trent, M. C. 2012. Development and use of a simple test method to evaluate reheat cracking sensitivity in the weld deposit region of a submerged arc weld. Master's thesis, University of Tennessee.
26. Zhang, L., et al. 2020. Method and criteria to evaluate reheat cracking susceptibility. *Welding Journal* 99(6): 175-s to 83-s.
27. Veron, P., Hipplesley, C. A., and Knott, J. F. 1984. Comparative studies of stress-relief cracking in relaxation test specimens and in a full-scale weldment. *International Journal of Pressure Vessels and Piping* 16: 29–51.
28. Saito, N., Komai, N., and Hashimoto, K. 2018. Evaluation of stress relaxation cracking susceptibility in alloy 617 for advanced USC boilers. *International Journal of Pressure Vessels and Piping* 168: 183–190.
29. Kuhn, B., et al. 2013. Stress-relaxation cracking test for welded joints. *Journal of Testing and Evaluation* 41(2): 207–216.
30. Kuhn, B., et al. 2013. An advanced method for evaluation of strain-age / stress-relaxation cracking susceptibility of welded joints. *Journal of Testing and Evaluation*, p. 1–25.
31. Wang, J., and Yu, S. 2022. Study on susceptibility and mechanism of reheat cracking in welded joint of Type 347 austenitic stainless steel. *International Journal of Chemical Engineering*, p. 1–12.
32. Christoffel, R. J. 1960. Notch-rupture strength of Type 347 heat-affected zone. *Welding Journal* 19(7): 315-s to 320-s.
33. Christoffel, R. J. 1963. Notch sensitivity of the heat-affected zone in Type 316 material. *Welding Journal* 22(1): 25s–28s.
34. McKeown, D. 1971. Re-heat cracking in high nickel alloy heat-affected zones. *Welding Journal* 50(5): 201-s to 206-s.
35. Howard, R. D. and Gooch, T. G. 1972. Reheat cracking in austenitic stainless steels Part 3 - The use of creep test principles. *The Welding Institute Research Bulletin* 13(6): 177–179.
36. Auzoux, Q., et al. 2000. Reheat cracking in austenitic stainless steels.
37. Pickle, T., et al. 2024. Stress relaxation cracking susceptibility evaluation in 347H stainless steel welds. *Welding in the World* 68: 657–667.
38. Fink, C., et al. 2020. Filler metal 16-8-2 for structural welds on 304H and 347H stainless steels for high temperature service. *Welding Journal* 99(12): 312-s to 322-s.
39. Kant, R. and DuPont, J. 2019. Stress relief cracking susceptibility in high-temperature alloys. *Welding Journal* 98(2): 29-s to 49-s.
40. Lee, H. S., Kim, B. S., and Hong, S. I. 2022. Comparison of stress relaxation cracking susceptibility of austenitic stainless steels. *Welding Journal* 101(9): 225-s to 239-s.
41. Purazrang, K. 1976. Fracture mechanics testing method for assessing susceptibility to stress-relief cracking. *Welding Journal*, p. 83-s to 88-s.
42. Turski, M., et al. 2008. Residual stress driven creep cracking in AISI Type 316 stainless steel. *Acta Materialia* 56: 3598–3612.
43. Auzoux, Q., et al. 2010. Effect of pre-strain on creep of three AISI 316 austenitic stainless steels in relation to reheat cracking of weld heat-affected zones. *Journal of Nuclear Materials* 400: 127–137.
44. Shiratti, A. M., et al. 2013. A new method of introducing long range residual stresses to study creep crack initiation. *13th International Conference on Fracture*, 1–10.
45. Smith, D. J., and Shirahatti, A. 2015. The effects of long-range residual stress, elastic follow-up and applied load on creep crack incubation and material toughness. *Journal of Strain Analysis*, p. 1–15.
46. Xiao, X., et al. 2022. Microstructural evolution and stress relaxation cracking mechanics for Super304H austenitic stainless steel weld metal. *Journal of Materials Science & Technology* 100: 82–90.
47. Py-Renaude, B., et al. 2023. Effect of welding microstructure on stress relaxation cracking by controlled residual stress generation in a 316L(N) austenitic stainless steel. *Metallurgical and Materials Transactions A* 54: 4650–4670.
48. Rehman, N., and Spindler, M. W. 2017. Notched bar creep of Type 316H at 550°C; Testing and finite element analysis. *4th International ECCO Conference*, 1–10.
49. Hares, E., et al., 2019. Repeat stress relaxation of notched bars and the dependence of creep damage on the relaxation rate. *International Journal of Pressure Vessels and Piping* 169: 115–124.
50. Nomura, K., and Kubushiro, K. 2022. Evaluation of reheat cracking susceptibility in high strength austenitic stainless steels. *Materials Transactions* 63(6): 877–882.
51. Spindler, M. W. 2019. How to prevent the initiation of cracks in elevated temperature plant - The gap between design and life assessment. *EDF Energy*, 1–34.
52. Bridgman, P. W. 1952. *Studies in large plastic flow and fracture: with special emphasis on the effects of hydrostatic pressure*. New York: McGraw Hill.
53. Hancock, J. W., and Mackenzie, A.C. 1976. On the mechanisms of ductile failure in high-strength steels subjected to multi-axial stress-states. *Journal of Mechanics and Physical Solids* 24: 147–169.
54. Skala, R. 2024. Interactive instruments. Retrieved from interactiveinstruments.com/materialtesters/.
55. Allegheny Ludlum. *Technical data blue sheet - Stainless steels*. Retrieved from metserve.co.za/pdf/al321.pdf.
56. Spindler, M. W. 2019. *Materials Issues in Advanced Gas Cooled Reactors*. McReynolds, R., ed. British Energy. p. 1–55.
57. Andren, H. O., Henjered, A., and Norden, H. 1980. Composition of MC precipitates in a titanium stabilized austenitic stainless steel. *Journal of Materials Science* 15: 2365–2368.
58. Andren, H. O., Henjered, A. and Karlsson, L. 1985. MX precipitates in stabilized austenitic stainless steels. *Stainless Steels*, p. 91–96.
59. Sourmail, T. 2001. Precipitation in creep resistant austenitic stainless steel. *Materials Science and Technology* 15: 1–15.
60. Powell, D. J., Pilkington, R., and Miller, D.A. 1988. The precipitation characteristics of 20%Cr/25%Ni-Mb stabilized stainless steel. *Acta Metallurgica* 36(3): 713–724.
61. NIMS Creep Data Sheet. 2003. *Metallographic Atlas of Long-Term Crept Materials No. M-2*. N.I.f.M.S. (NIMS), Editor.
62. Yang, Y. 2023. Stress relaxation cracking in 347H austenitic stainless steel weldments under various heat treatments: Experiments and Modeling. PhD diss., University of Tennessee.
63. Kim, D., et al. 2024. Effect of metastable precipitate phase transformation on reheat cracking in SS347H welding. *Engineering Failure Analysis* 164(10): 108603.
64. Spindler, M. W. 2004. The multiaxial creep ductility of austenitic stainless steels. *Fatigue and Fracture of Engineering Structures* 27: 273–281.
65. Nibkin, K. 2017. A unified multiscale ductility exhaustion based approach to predict uniaxial, multiaxial creep rupture and crack growth. *Engineering Fracture Mechanics* 179: 240–259.
66. Sandstrom, R. 2024. *Basic modeling and theory of creep in metallic materials*. Springer.
67. Ren, W., and Lin, L. 2019. Consideration of thermal embrittlement in alloy 316H for advanced non-light water reactor applications. *ASME 2019 Pressure Vessels and Piping Conference*.

GEORGE A. YOUNG (young@kairospower.com), **ANDREW BRITTAN**, **ANDREW DONG**, **KYNA CHEN**, and **NICK NGUYEN** are with Kairos Power LLC, Alameda, Calif.